

**Spin Seebeck effect in  $\text{Cu}_2\text{OSeO}_3$ : Test of bulk magnon spin current theory**A. Akopyan,<sup>1</sup> N. Prasai,<sup>1,\*</sup> B. A. Trump<sup>Ⓧ</sup>,<sup>2,3,†</sup> G. G. Marcus,<sup>3</sup> T. M. McQueen,<sup>2,3,4</sup> and J. L. Cohn<sup>Ⓧ</sup>,<sup>1,‡</sup><sup>1</sup>*Department of Physics, University of Miami, Coral Gables, Florida 33124, USA*<sup>2</sup>*Department of Chemistry, Johns Hopkins University, Baltimore, Maryland 21218, USA*<sup>3</sup>*Department of Physics and Astronomy, Institute for Quantum Matter, Johns Hopkins University, Baltimore, Maryland 21218, USA*<sup>4</sup>*Department of Material Science and Engineering, Johns Hopkins University, Baltimore, Maryland 21218, USA*

(Received 9 December 2019; accepted 24 February 2020; published 23 March 2020)

We report measurements of the low-temperature ( $T \leq 15$  K) longitudinal spin Seebeck coefficient ( $S_{LSE}$ ) in bulk single crystals of the helimagnetic insulator  $\text{Cu}_2\text{OSeO}_3$  with Pt contacts. Simultaneous measurement of both  $S_{LSE}$  and the magnon thermal conductivity ( $\kappa_m$ ) demonstrates their correlation and allows for quantitative and favorable comparison to bulk magnon spin current theory.

DOI: [10.1103/PhysRevB.101.100407](https://doi.org/10.1103/PhysRevB.101.100407)

Magnon transport and energy exchange between magnons and phonons are central to the growing fields of spin caloritronics [1] and magnon spintronics [2]. Crucial to potential applications is the conversion of thermally driven spin currents in a magnetic insulator to an electrical signal via the inverse spin Hall effect in a heavy-metal thin film in interfacial contact—the spin Seebeck effect. Considerable experimental and theoretical development has focused on studies of Pt contacts to the insulating ferrimagnet yttrium-iron garnet (YIG).

Magnon spin current theory for the bulk spin Seebeck effect [3–5] implies a direct relationship between the longitudinal spin Seebeck coefficient ( $S_{LSE}$ ) and magnon thermal conductivity ( $\kappa_m$ ). Quantitative tests of this relationship have not been possible in any material because  $\kappa_m$  is not typically large enough or easily separable from the lattice thermal conductivity. Though  $\kappa_m$  has been determined for YIG at low temperature in applied magnetic field [6–8], it is not clearly correlated with  $S_{LSE}$  (e.g., their maxima appear to occur at very different temperatures [9,10]).

Recent studies [11] demonstrated that  $\text{Cu}_2\text{OSeO}_3$ , a helimagnetic insulator with  $T_C = 58$  K, harbors the largest known  $\kappa_m$  for any ferro- or ferrimagnetic insulator, with a maximum  $\kappa_m \sim 60$ – $80$  W/mK at  $T \simeq 5$ – $6$  K. Here we report on measurements of  $S_{LSE}$  in 10-nm Pt/bulk single-crystal  $\text{Cu}_2\text{OSeO}_3$  heterostructures with which  $\kappa_m$ , measured simultaneously, is well correlated. The data, which include interfacial spin-mixing conductances varying by more than an order of magnitude, are in quantitative agreement with the predictions of bulk spin current theory.

$\text{Cu}_2\text{OSeO}_3$  comprises a three-dimensional distorted pyrochlore (approximately fcc) lattice of corner-sharing Cu

tetrahedra [12,13]. Strong magnetic interactions within tetrahedra lead to a 3-up–1-down, spin  $S = 1$  magnetic state [14,15] with weaker interactions between tetrahedra leading to their ferromagnetic ordering [16,17] below  $T_C \simeq 58$  K. At low temperatures [18] the low-field state [inset, Fig. 1(a)] includes multiple helical ( $H$ ) domains (aligned along the  $\langle 100 \rangle$  easy-axis directions) wherein atomic spins rotate within a plane perpendicular to the helical axis with a wavelength  $\lambda_h \simeq 62$  nm. At  $H \gtrsim 10$ – $25$  mT (depending on field orientation) the helices of individual domains rotate along the field to form a single-domain, conical phase ( $C$ ). For  $H \gtrsim 50$ – $75$  mT the ferrimagnetic, fully polarized ( $FP$ ) state emerges.

Phase pure, single crystals of  $\text{Cu}_2\text{OSeO}_3$  were grown by chemical vapor transport as described elsewhere [11,19]. Specimens were cut from single-crystal ingots, oriented by x-ray diffraction, and polished into thin parallelepipeds. A two-thermometer, one-heater method was employed to measure the spin Seebeck effect (using 25- $\mu\text{m}$ -diam. Au wires) and thermal conductivity simultaneously. A sputtered Pt film (10 nm thick) was deposited onto the heater end of the crystal and isolated from the heater with varnish. Further details on the measurements, crystal polishing/etching [20–21], and properties of the Pt films are discussed in the Supplemental Material [22].

We focus in this work on data for three specimens, all with heat flow along the  $[111]$  direction and magnetic field along  $[1\bar{1}0]$  [inset, Fig. 1(a)]. Crystal 1 is the same crystal ( $5 \times 1.10 \times 0.26$  mm<sup>3</sup>) for which thermal conductivity data were reported in Ref. [11]. This crystal was subsequently cut, polished (new cross-sectional area  $A = 0.86 \times 0.20$  mm<sup>2</sup>), prepared with a fresh Pt film, and remeasured. This second data set is the primary focus of the narrative since it is most extensive and because its SSE signal was a factor of 4–5 larger than during the first experiment. The two specimens are distinguished by their transverse dimensions,  $\ell_0 = 0.60$  mm and 0.47 mm, respectively, where  $\ell_0 \equiv 2\sqrt{A/\pi}$ . A second crystal with  $\ell_0 = 0.31$  mm ( $A = 0.70 \times 0.11$  mm<sup>2</sup>; crystal 5 from Ref. [11]) was also studied. Data for the  $\ell_0 = 0.60$  mm and  $\ell_0 = 0.31$  mm specimens are included in Fig. 3 and more extensive data in Supplemental Material Figs. S4 and S5 [22].

\*Present address: Department of Physics, St. Mary's College of Maryland, St. Mary's City, MD 20686.

†Present address: NIST Center for Neutron Research, National Institute of Standards and Technology, Gaithersburg, Maryland 20899-6102.

‡Corresponding author: [jjohn@miami.edu](mailto:jjohn@miami.edu)

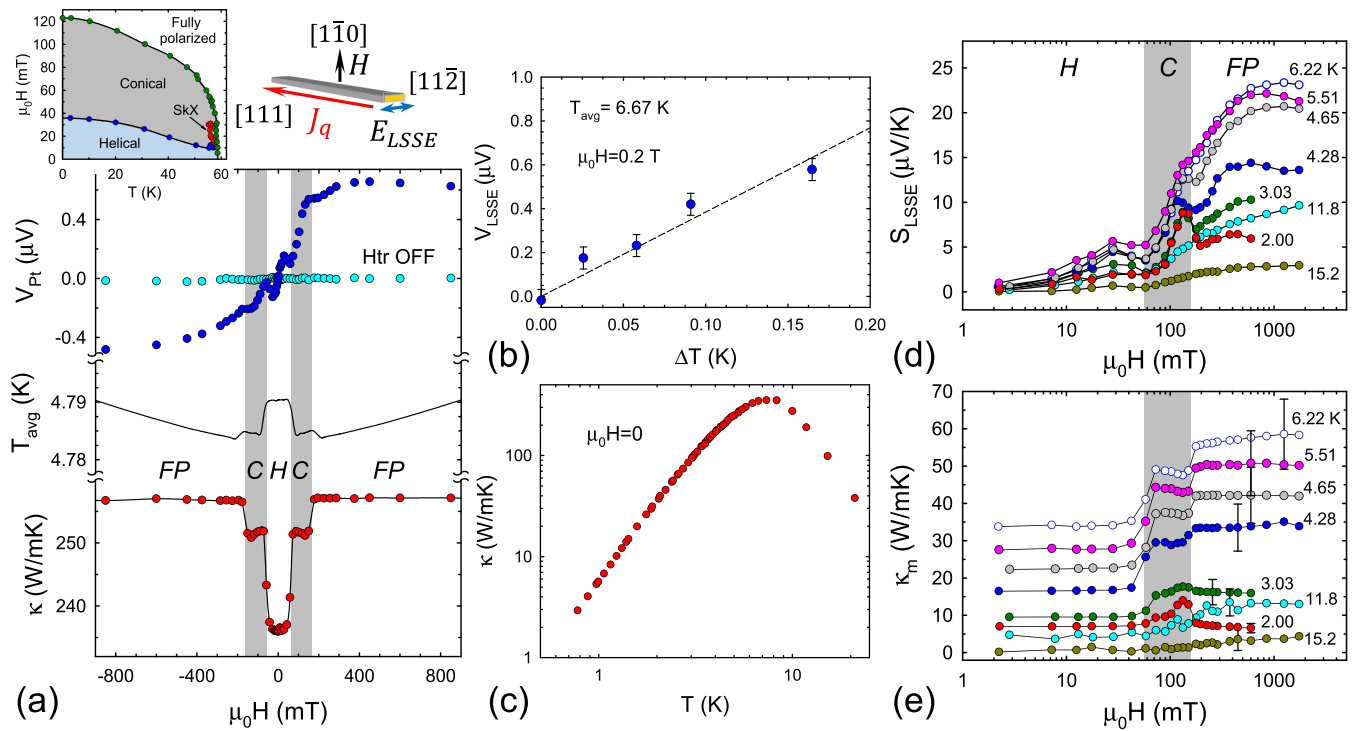


FIG. 1. (a) From top to bottom: Spin Seebeck voltage (for heater on and off), average temperature, and thermal conductivity vs applied field at  $T_{\text{avg}} = 4.79$  K. Left inset: Magnetic phase diagram (adapted from Ref. [18]); right inset: Orientation of heat flow and fields. (b) SSE voltage vs  $\Delta T$  at 6.67 K, (c) zero-field  $\kappa(T)$ , (d) SSE coefficient, and (e) magnon thermal conductivity vs applied field for various temperatures. Error bars are discussed in the text and in Ref. [11]. The shading in (a), (d), and (e) distinguishes the conical (C) spin phase from helical (H) and fully polarized (FP) phases at lower and higher field, respectively.

Given the high thermal conductivity of  $\text{Cu}_2\text{OSeO}_3$  [11] and the desire to maximize length along the inverse spin Hall field ( $[11\bar{2}]$ ), long, thin parallelepiped specimens were necessary, leading to large demagnetization factors ( $N \sim 0.75$ ) and some nonuniformity of the applied field; we report external field values here. Extensive prior measurements of  $M(H)$  and  $\kappa(H)$  on crystals [11,23] with small  $N$  reveal consistent, coincident signatures of the spin-phase transitions that are employed here to identify the phase boundaries from  $\kappa(H)$  data.

Prior work demonstrates that field-dependent changes in  $\kappa$  are entirely magnonic [11,23]. Separation of  $\kappa_L$  and  $\kappa_m$  is possible for  $T \lesssim 1.2$  K where the high-field condition  $E_H \gg k_B T$  is met ( $E_H = g\mu_B H$ , the Zeeman energy) and thus spin-wave excitations are depopulated (gapped). The mean free paths for both phonons and magnons are comparable to  $\ell_0$  at  $T \lesssim 2$  K. At higher  $T$  where field suppression of  $\kappa_m$  is incomplete, Callaway model fitting is employed to estimate  $\kappa_L$ , with  $\kappa_m$  computed by subtraction [11,22].

Figure 1(a) shows the field dependence of, from top to bottom, the Pt film voltage (with a constant offset voltage subtracted), average specimen temperature, and thermal conductivity at  $T_{\text{avg}} = 4.79$  K. The null Pt voltage during the same sweep with the heater off is also shown. Figure 1(b) confirms linearity in  $\Delta T$  of the antisymmetrized spin Seebeck voltage,  $V_{\text{LSSE}} = [V_{\text{Pt}}(H) - V_{\text{Pt}}(-H)]/2$ , and Fig. 1(c) shows the zero-field  $\kappa(T)$ .  $\kappa(H)$  exhibits a step-like increase at the  $H$ - $C$  spin-phase transition, a plateau within the  $C$  phase, and another step-like increase at the  $C$ - $FP$  phase boundary. Similar features for various orientations

of heat flow and applied field have been reported in prior studies [11,23].

Figure 1(d) shows the longitudinal spin Seebeck coefficient as a function of field at selected temperatures,  $S_{\text{LSSE}} = (V_{\text{LSSE}}/\Delta T)(l/w)$ , where  $l$  is the distance between thermometers along the heat flow and  $w$  is the length of the Pt film (approximately the specimen width). Figure 1(e) shows the magnon thermal conductivity computed by subtracting a field-independent  $\kappa_L$ . The error bars reflect uncertainties in estimating  $\kappa_L$  from the model fitting and are largest at  $T \sim 7$  K where  $\kappa(T)$  has its maximum [11,22]. Similar  $S_{\text{LSSE}}(H)$  and  $\kappa_m(H)$  data for the other specimens are presented in Figs. S4 and S5 [22].

$S_{\text{LSSE}}(H)$  exhibits a small maximum at fields below the  $H$ - $C$  phase transition, presumably associated with partial reorientation of the three  $\langle 100 \rangle$ -oriented helical domains, established in zero-field cooling. A sharp increase in  $S_{\text{LSSE}}(H)$  characterizes the transition to the conical phase, following the increase in  $\kappa_m(H)$ . At  $T \gtrsim 6$  K,  $S_{\text{LSSE}}(H)$  increases smoothly through the  $C$ - $FP$  transition, and saturates or declines in magnitude within the  $FP$  phase. For lower  $T$  an inflection appears at the  $C$ - $FP$  transition and a steplike decrease emerges, becoming more prominent at the lowest  $T$ . This latter feature coincides with a steplike decrease in  $\kappa_m(H)$  (see data for 3.03 and 2.00 K), and thus can be attributed to the effects of a larger spin gap (estimated in the analysis below as  $\Delta \sim 0.3$  meV [22]) within the  $FP$  phase (the spin gap in the conical phase is quite small [24],  $\sim 12$   $\mu\text{eV}$ ). A fraction of the thermal magnons thus become gapped as the field increases through the  $C$ - $FP$

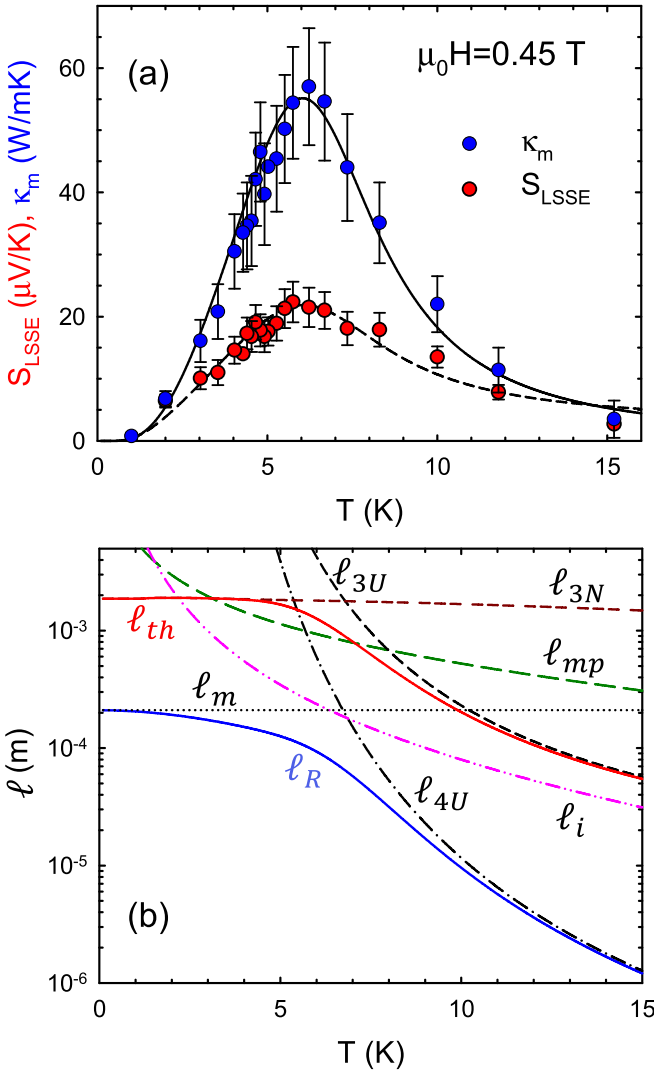


FIG. 2. (a)  $\kappa_m(T)$  and  $S_{LSSE}(T)$  in the fully polarized phase at  $\mu_0H = 0.45$  T. Error bars for  $\kappa_m$  are described in the text, and for  $S_{LSSE}$  are dictated by uncertainty in the geometric factor (20%). The solid curve is computed from Eq. (1) and the dashed curve from Eq. (2) with  $\tau_{th} = (\tau_{3N}^{-1} + \tau_{mp}^{-1} + \tau_{3U}^{-1})^{-1}$  (see text). (b) Thermally averaged scattering lengths computed from the model of Ref. [30] (see also the Supplemental Material [22]).

transition, effectively removing their contribution to  $\kappa_m$ . That the effects of the spin gap opening are evidenced in  $S_{LSSE}$  at higher  $T$  than for  $\kappa_m$  suggests that *subthermal* magnons contribute some weight to the spin Seebeck effect, as has been proposed to understand the field-induced suppression of the SSE in YIG [9,25,26].

The most significant observation from Figs. 1(d) and 1(e) and the principal result of this work, is the clear correspondence between  $\kappa_m$  and  $S_{LSSE}$ ; Fig. 2(a) illustrates this correspondence in  $T$  at fixed field  $\mu_0H = 0.45$  T, within the *FP* phase where  $S_{LSSE}$  is near its maximum value. As a first test of theory, we demonstrate that the same magnon relaxation rate, employed in prior work to model  $\kappa_m(T)$  for crystal 1 and other similar crystals [11], also describes  $S_{LSSE}(T)$ .

Inelastic neutron scattering studies [27] indicate a single spin-wave branch relevant to magnon transport at low  $T$  in

TABLE I. Magnon scattering and spin Seebeck parameters.

Specimen	$\ell_0$ (mm)	$c$ (ppm)	$\ell_m$ (mm)	$R_N$ ( $\Omega$ )	$g_{\text{eff}}^{\uparrow\downarrow}$ ( $10^{15} \text{ m}^{-2}$ )
Crystal 1	0.60	22	0.30	467	2.45
"	0.47	22	0.21	120	39.3
Crystal 2	0.31	44	0.18	293	1.27

$\text{Cu}_2\text{OSeO}_3$  that is well described by an isotropic dispersion [28],  $E = \Delta + g\mu_B H + \hbar\omega_{ZB}[1 - \cos(\pi q)]$ , with  $\hbar\omega_{ZB} = 4.55$  meV and  $q = k/k_m$  the reduced wave number ( $k_m$  is the maximum wave number). The magnon thermal conductivity and spin Seebeck coefficient from Boltzmann theory can be written as [3–5]

$$\kappa_m = \frac{k_B k_m^3}{6\pi^2} \tau_R B_{21}, \quad (1)$$

$$S_{LSSE} = R_N \lambda_N \frac{2e}{\hbar} \theta_{SH} (\tau_m \tau_{th})^{1/2} \frac{B_{11} C_2}{(B_{10} C_1)^{1/2}} F g_{\text{eff}}^{\uparrow\downarrow}, \quad (2)$$

where  $B_{ij}$  and  $C_k$  are the integrals,

$$B_{ij} = \int_0^1 dq q^2 v_m^2 \frac{x^i (e^x)^j}{(e^x - 1)^{1+j}}, \quad C_k = \int_0^1 dq q^2 \frac{x^k}{(e^x - 1)},$$

$$F = \frac{\hbar \gamma k_B k_m^3}{4\pi M_S \pi^2 \sqrt{3}},$$

$v_m = (1/\hbar)dE/dk$  is the magnon velocity;  $x = E/k_B T$ ;  $R_N$ ,  $\lambda_N = 3.7$  nm and  $\theta_{SH} = 0.05$  are the Pt film resistance, spin-diffusion length, and spin Hall angle [5];  $\gamma = 1.82 \times 10^{11} \text{ T}^{-1} \text{ s}^{-1}$  is the gyromagnetic ratio [29]; and  $4\pi M_S \simeq 1.15 \times 10^5$  A/m is the saturation magnetization [18]. The integrals are performed over a spherical Brillouin zone with  $(4/3)\pi k_m^3 = (2\pi/a)^3$ . We employ thermally averaged scattering times for which the momentum dependence has already been integrated out.

The transport relaxation rate ( $\tau_R^{-1}$ ) incorporates magnon-magnon umklapp (3U, 4U), magnon-impurity (i), and magnon-boundary (b) scattering,  $\tau_R^{-1} = \tau_{3U}^{-1} + \tau_{4U}^{-1} + \tau_i^{-1} + \tau_b^{-1}$ , computed for an isotropic Heisenberg model with quadratic magnon dispersion [30]. The expressions rely on four parameters, two of which are fixed by the value of the lattice constant and  $T_C$  [11,22]. The strength of impurity and boundary terms are set by the nonmagnetic impurity concentration ( $c$ ) and magnetic domain size  $\ell_m \leq \ell_0$  ( $\tau_b = \ell_m/\langle v_m \rangle$ , with  $\langle v_m \rangle$  the momentum-averaged magnon velocity [22]). The latter, employed here as a fitting parameter, was determined directly in Ref. [11] from the  $\kappa_m \propto T^2$  behavior observed within the *C* phase at low  $T$  as  $\sim 0.30$  mm for the specimen with  $\ell_0 = 0.60$  mm. The solid curve in Fig. 2(a) demonstrates good agreement with  $\kappa_m$  using the  $T$ -dependent scattering lengths ( $\ell_j = \langle v_m \rangle \tau_j$ ) shown in Fig. 2(b). Similar quality fitting curves for the other specimens are shown in Figs. S4 and S5 [22]; Table I summarizes the parameters.

Two relaxation times are distinguished in Eq. (2) for the SSE coefficient, characterizing scattering that conserves (does not conserve) magnon number,  $\tau_m$  ( $\tau_{th}$ ) [31]; the magnon diffusion length and the SSE signal are proportional to  $\sqrt{\tau_m \tau_{th}}$ , where  $\tau_m \ll \tau_{th}$ . We take  $\tau_m = \tau_R$ , as  $\tau_R$  is dominated by magnon-conserving processes given that  $\tau_{3U} \ll \tau_{4U}$

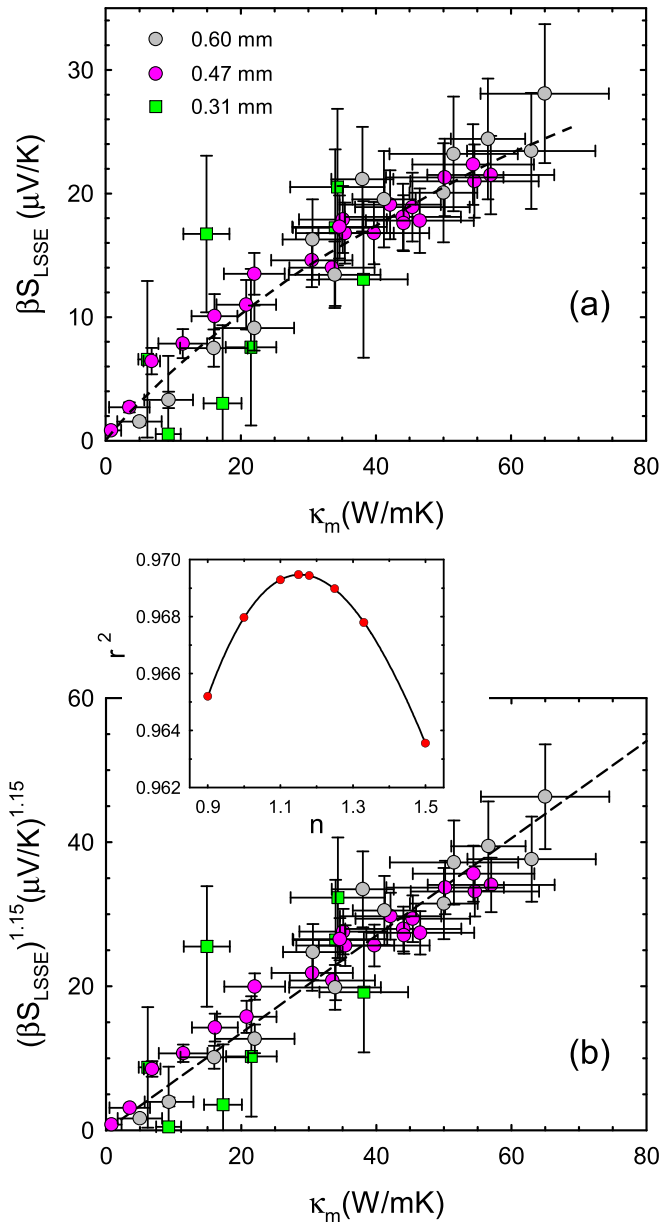


FIG. 3. Correlation between  $S_{LSSE}$  and  $\kappa_m$  in the fully polarized phase ( $\mu_0 H = 0.45 T$ ) for all three specimens on linear (a) and power-law (b) scaling. Data for crystal 1 with  $\ell_0 = 0.60$  mm and crystal 2 ( $\ell_0 = 0.31$  mm) have been rescaled by their values of  $R_N g_{\text{eff}}^{\uparrow\downarrow}$  (Table I) to match that of crystal 1 with  $\ell_0 = 0.47$  mm as described in the text. The dashed line in (a) is a guide and in (b) a linear least-squares fit. The inset shows the quality of the power-law fit to be maximized for  $n = 1.15$ .

[Fig. 2(b)]. Note that magnon-phonon interactions (characterized by  $\tau_{mp}$ ), which do not conserve magnon number (two-magnon, one-phonon interactions are predominant), are weak in the low- $T$  regime relevant here [30,32] and play little role in  $\kappa_m$  provided there is sufficient coupling to ensure energy from the heater (coupling only to phonons) enters the magnon system. The criterion for this [33],  $\tau_{mp} \gtrsim \ell_0/v_{ph}$  ( $v_{ph} \simeq 2$  km/s is the phonon velocity [11,22]), is satisfied [11] using  $\tau_{mp}$  estimated from the intrinsic ferromagnetic resonance linewidth [29] [Fig. 2(b)]. With  $\tau_m = \tau_R$  fixed by fitting to  $\kappa_m(T)$  and  $\tau_{th}^{-1} = \tau_{mp}^{-1} + \tau_{3N}^{-1} + \tau_{3U}^{-1}$ ,  $g_{\text{eff}}^{\uparrow\downarrow}$  was adjusted to produce good agreement with  $S_{LSSE}$  [dashed curve in Fig. 2(a) and Figs. S4 and S5 for the other specimens].

The  $T$  dependence arising from the relaxation times for  $S_{LSSE}$  differs from that for  $\kappa_m$  by the factor  $(\tau_{th}/\tau_R)^{1/2}$ , which is weakly  $T$  dependent over the investigated range [Fig. S6(a)]. This observation motivates a more fundamental test of the theory, independent of the relaxation times—Eqs. (1) and (2) predict the two transport coefficients to be directly related through their integral expressions. A *sublinear* relationship between  $S_{LSSE}$  and  $\kappa_m$  for all specimens emerges when the spin Seebeck coefficients are rescaled by plotting  $\beta S_{LSSE}$  against  $\kappa_m$  [Fig. 3(a)], where  $\beta$  is the ratio of  $R_N g_{\text{eff}}^{\uparrow\downarrow}$  for the  $\ell_0 = 0.47$  mm specimen to that for the others:  $\beta = 4.1$  (12.7) for  $\ell_0 = 0.60$  (0.31) mm specimens. Figure 3(b) demonstrates that a power-law relation,  $(S_{LSSE})^n \propto \kappa_m$ , provides a good description of the data with  $n = 1.15$  providing the best fit [inset, Fig. 3(b)]. In Fig. S6(b) we demonstrate that the integrals follow the relationship  $B_{11}C_2/(B_{10}C_1)^{1/2} \propto (B_{21})^{0.852}$  over most of the  $T$  range, yielding  $n = (1/0.852) \simeq 1.17$  in excellent agreement with the data.

In summary, the unprecedentedly large magnon thermal conductivity of  $\text{Cu}_2\text{OSeO}_3$  and simultaneous measurement of spin Seebeck coefficient have allowed for new quantitative tests affirming bulk magnon spin current theory. These results highlight this compound as a model system for the study of magnon interactions and their role in the transport of spin and heat.

Work at the University of Miami was supported by the U.S. Department of Energy (DOE), Office of Science, Basic Energy Sciences (BES), under Award No. DE-SC0008607. T.M.M. was supported as part of the Institute for Quantum Matter, an Energy Frontier Research Center funded by the U.S. DOE, Office of Science, BES under Award No. DE-SC0019331. B.A.T. acknowledges the NSF, Division of Materials Research, Solid State Chemistry, CAREER Grant No. DMR-1253562. G.G.M. acknowledges generous support from the NSF-GRFP, Grant No. DGE-1232825.

- [1] Stephen R. Boona, Roberto C. Myers, and Joseph P. Heremans, *Energy Environ. Sci.* **7**, 885 (2014).
- [2] A. V. Chumak, V. I. Vasyuchka, A. A. Serga, and B. Hillebrands, *Nat. Phys.* **11**, 453 (2015).
- [3] Steven S.-L. Zhang and S. Zhang, *Phys. Rev. Lett.* **109**, 096603 (2012); *Phys. Rev. B* **86**, 214424 (2012).

- [4] S. M. Rezende, R. L. Rodríguez-Suárez, R. O. Cunha, A. R. Rodrigues, F. L. A. Machado, G. A. Fonseca Guerra, J. C. Lopez Ortiz, and A. Azevedo, *Phys. Rev. B* **89**, 014416 (2014).
- [5] S. M. Rezende, R. L. Rodríguez-Suárez, R. O. Cunha, J. C. López Ortiz, and A. Azevedo, *J. Magn. Magn. Mater.* **400**, 171 (2016).



- [6] B. Luthi, *J. Phys. Chem. Solids* **23**, 35 (1962).
- [7] R. L. Douglass, *Phys. Rev.* **129**, 1132 (1963).
- [8] S. R. Boona and J. P. Heremans, *Phys. Rev. B* **90**, 064421 (2014).
- [9] H. Jin, S. R. Boona, Z. Yang, R. C. Myers, and J. P. Heremans, *Phys. Rev. B* **92**, 054436 (2015).
- [10] R. Iguchi, Ken-ichi Uchida, S. Daimon, and E. Saitoh, *Phys. Rev. B* **95**, 174401 (2017).
- [11] N. Prasai, B. A. Trump, G. G. Marcus, A. Akopyan, S. X. Huang, T. M. McQueen, and J. L. Cohn, *Phys. Rev. B* **95**, 224407 (2017).
- [12] P. G. Meunier and M. Bertaud, *J. Appl. Crystallogr.* **9**, 364 (1976).
- [13] H. Effenberger and F. Pertlik, *Monatsh. Chem.* **117**, 887 (1986).
- [14] Jan-Willem G. Bos, C. V. Colin, and T. T. M. Palstra, *Phys. Rev. B* **78**, 094416 (2008).
- [15] M. Belesi, I. Rousochatzakis, H. C. Wu, H. Berger, I. V. Shvets, F. Mila, and J. P. Ansermet, *Phys. Rev. B* **82**, 094422 (2010).
- [16] J. Romhányi, J. van den Brink, and I. Rousochatzakis, *Phys. Rev. B* **90**, 140404(R) (2014).
- [17] M. Ozerov, J. Romhányi, M. Belesi, H. Berger, J.-Ph. Ansermet, J. van den Brink, J. Wosnitza, S. A. Zvyagin, and I. Rousochatzakis, *Phys. Rev. Lett.* **113**, 157205 (2014).
- [18] T. Adams, A. Chacon, M. Wagner, A. Bauer, G. Brandl, B. Pedersen, H. Berger, P. Lemmens, and C. Pfleiderer, *Phys. Rev. Lett.* **108**, 237204 (2012).
- [19] J. Panella, B. A. Trump, G. G. Marcus, and T. M. McQueen, *Cryst. Growth Des.* **17**, 4944 (2017).
- [20] A. Aqeel, N. Vlietstra, A. Roy, M. Mostovoy, B. J. van Wees, and T. T. M. Palstra, *Phys. Rev. B* **94**, 134418 (2016).
- [21] M. B. Jungfleisch, V. Lauer, R. Neb, A. V. Chumak, and B. Hillebrands, *Appl. Phys. Lett.* **103**, 022411 (2013); S. Pütter, S. Geprägs, R. Schlitz, M. Althammer, A. Erb, R. Gross, and S. T. B. Goennenwein, *ibid.* **110**, 012403 (2017).
- [22] See Supplemental Material at <http://link.aps.org/supplemental/10.1103/PhysRevB.101.100407> for additional details regarding specimen preparation, data for other specimens, and analysis, which includes Refs. [34–39].
- [23] N. Prasai, A. Akopyan, B. A. Trump, G. G. Marcus, S. X. Huang, T. M. McQueen, and J. L. Cohn, *Phys. Rev. B* **99**, 020403(R) (2019).
- [24] M. I. Kobets, K. G. Dergachev, E. N. Khatsko, A. I. Rykova, P. Lemmens, D. Wulferding, and H. Berger, *Low Temp. Phys.* **36**, 176 (2010).
- [25] T. Kikkawa, Ken-ichi Uchida, S. Daimon, Zhiyong Qiu, Y. Shiomi, and E. Saitoh, *Phys. Rev. B* **92**, 064413 (2015).
- [26] I. Diniz and A. T. Costa, *New J. Phys.* **18**, 052002 (2016).
- [27] P. Y. Portnichenko, J. Romhányi, Y. A. Onykienko, A. Henschel, M. Schmidt, A. S. Cameron, M. A. Surmach, J. A. Lim, J. T. Park, A. Schneidewind, D. L. Abernathy, H. Rosner, J. van den Brink, and D. S. Inosov, *Nat. Commun.* **7**, 10725 (2016).
- [28] Helimagnon excitations influence only the very low energy dispersion, corresponding to wave numbers ( $k < k_h = 2\pi/\lambda_h \simeq 0.01 \text{ \AA}^{-1}$ ) and energies far below those of the thermal magnons relevant to the present experiments (see Ref. [27]). Furthermore, our analysis pertains to data within the fully polarized, collinear magnetic state where helimagnetic effects are absent.
- [29] S. Seki, Y. Okamura, K. Kondou, K. Shibata, M. Kubota, R. Takagi, F. Kagawa, M. Kawasaki, G. Tatara, Y. Otani, and Y. Tokura, *Phys. Rev. B* **93**, 235131 (2016).
- [30] J.-J. Forney and J. Jäckle, *Phys. Kondens. Materie* **16**, 147 (1973).
- [31] L. J. Cornelissen, K. J. H. Peters, G. E. W. Bauer, R. A. Duine, and B. J. van Wees, *Phys. Rev. B* **94**, 014412 (2016).
- [32] A. I. Akhiezer, V. G. Bar'yakhtar, and M. I. Kaganov, *Sov. Phys. Usp.* **3**, 661 (1961).
- [33] D. J. Sanders and D. Walton, *Phys. Rev. B* **15**, 1489 (1977).
- [34] S. Y. Huang, X. Fan, D. Qu, Y. P. Chen, W. G. Wang, J. Wu, T. Y. Chen, J. Q. Xiao, and C. L. Chien, *Phys. Rev. Lett.* **109**, 107204 (2012); Y. M. Lu, Y. Choi, C. M. Ortega, X. M. Cheng, J. W. Cai, S. Y. Huang, L. Sun, and C. L. Chien, *ibid.* **110**, 147207 (2013).
- [35] Y. Shiomi, T. Ohtani, S. Iguchi, T. Sasaki, Z. Qiu, H. Nakayama, K. Uchida, and E. Saitoh, *Appl. Phys. Lett.* **104**, 242406 (2014).
- [36] See, e.g., N. Giordano and M. A. Pennington, *Phys. Rev. B* **47**, 9693 (1993), and references therein.
- [37] H. Hoffmann, F. Hofmann, and W. Schoepe, *Phys. Rev. B* **25**, 5563 (1982).
- [38] R. Berman, *Thermal Conduction in Solids* (Oxford University Press, Oxford, 1976).
- [39] P. B. Allen, *Phys. Rev. B* **88**, 144302 (2013).